On the design of bank revetments at inland waterways subjected to ship-induced water level drawdown
A probabilistic infinite slope analysis

Sorgatz, Julia; van den Eijnden, Abraham P.; Montenegro, Héctor; Hicks, Michael A.

Important note
To cite this publication, please use the final published version (if applicable).
Please check the document version above.

On the design of bank revetments at inland waterways subjected to ship-induced water level drawdown: A probabilistic infinite slope analysis

Julia Sorgatz[1], Abraham P. van den Eijnden[2], Héctor Montenegro[3], Michael A. Hicks[4]

Abstract

To protect embankments along German inland waterways against local slope sliding failure caused by ship-induced water level drawdown, they are mainly secured by bank revetments. Often, large embankment sections are designed on the basis of a limited number of field and laboratory tests. Thus, uncertainties arise with regard to the mechanical and hydraulic ground properties. Current design standards account for these uncertainties by conservative design assumptions and empirical knowledge. This paper investigates the effects of vertically non-homogeneous ground properties on the required armour layer thickness using 1D random fields and an infinite slope model, which was modified to account for ship-induced drawdowns. Within the limitations of the infinite slope assumptions, the effects of a spatially variable friction angle and hydraulic conductivity are investigated and compared to deterministic benchmark cases. The investigations show that the level of safety obtained with the deterministic design depends strongly on the choice of the characteristic values. Particularly, the hydraulic conductivity determines the reliability of the design. In some cases, the 5 % quantile of the hydraulic conductivity does not yield a conservative estimate of the required armour layer thickness. In the case of the effective friction angle, the 5 % quantile may overestimate the required armour layer thickness for permeable soils. For less permeable soils, the 5 % quantile meets the solution of the random field analyses. For the combination of random effective friction angle and random hydraulic conductivity, all investigated benchmark studies seem to ensure engineering safety, but on different reliability levels. Based on these findings, recommendations regarding site exploration and choice of characteristic values of hydraulic conductivity and effective friction angle are provided.

Keywords

slope stability, ship-induced drawdown, revetment design, non-homogeneous ground properties, random fields

1 Introduction

To ensure safety and ease of navigation, and to protect the adjacent terrain, sloped banks at inland waterways are commonly secured by bank protections. Revetments, which consist of a loose or grouted armour stones on a filter layer, are the most common bank protection type at German inland waterways. To protect the slope against erosion, the hydraulic design defines the minimum armour stone diameter necessary to withstand waves and currents. The geotechnical design evaluates the armour layer thickness required to ensure embankment stability under ship-induced drawdowns (Rock Manual, 2007; GBB, 2010). In the presented study the required armour layer thickness is investigated. Furthermore, this study focuses on canals where ship-induced loads govern the design.

When a vessel passes through the water in a waterway with a limited cross-section, a sequence of waves and currents is induced (see Figure 1). This paper deals with the ship-induced drawdown of the primary wave system. The drawdown results from the cross section reduction by the vessel which causes an increase in flow velocity and, thereby, a lowering of the water level next to the vessel (Gesing, 2010). For the design of the armour layer thickness, the ship-induced drawdown is crucial (GBB, 2010). If the water level is lowered faster than the pore pressure in the embankment soil can adapt to in order to achieve a new hydrostatic equilibrium, excess pore pressure may develop (Köhler, 1989). The excess pore pressure leads to a reduced effective stress which lowers the shear strength of the soil. This may result in a local slope sliding along a failure surface in the ground or soil liquefaction. The additional mass of the revetment increases the resistance of the embankment against sliding failure and liquefaction.
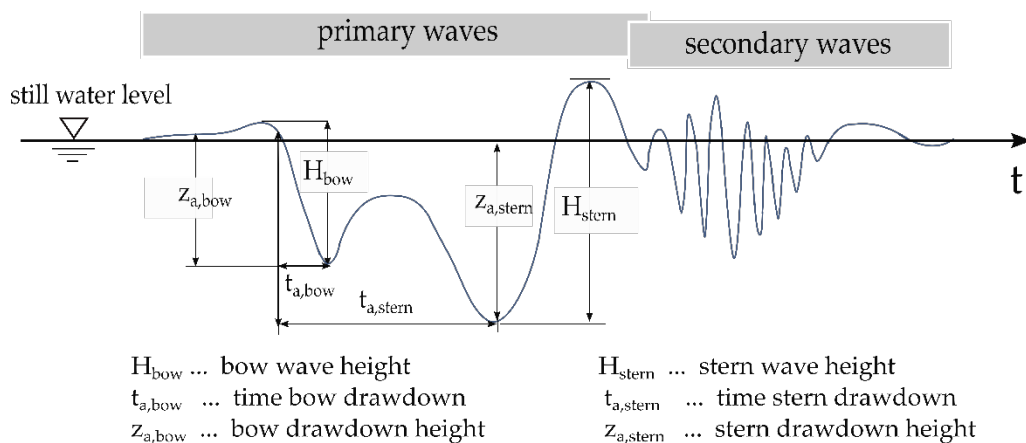
Figure 1: Schematic illustration of ship-induced drawdown heights at bow ($z_{a,bow}$) and stern ($z_{a,stern}$) and corresponding drawdown times ($t_{a,bow}$, $t_{a,stern}$) over time t (GBB 2010, cf. p. 62).

As in any geotechnical design, the choice of the characteristic values for revetment design, e. g., hydraulic conductivity k and friction angle ϕ', is affected by a number of uncertainties (e. g. Phoon et al., 2016): the spatial variability in the ground, errors and uncertainties as a consequence of the investigation method, the transformation models used and the statistically uncertainty resulting from a limited number of samples. At present, the analysis of embankment stability along German inland waterways is conducted with characteristic values which do not explicitly account for spatially variable soil conditions (GBB, 2010). Yet, it is assumed that the location and "layering" of permeable and less permeable zones in combination with a spatially variable shear strength may affect the embankment stability strongly. As a consequence, current design procedures may result in a design which is not always the most favourable in terms of safety, economic efficiency and ecology.

To investigate the effects of spatial variability of soils on slope stability, Griffiths et al. (2011) proposed a simplified probabilistic analysis using an infinite slope model and random field theory. Since then, various authors have applied this combination of an infinite slope analysis with random fields to investigate the stability of slopes with spatially variable soils under rainfall infiltration (Santoso et al., 2011; Cho, 2014; Zhang et al., 2014). An extension towards the analysis of unsaturated slopes is presented by Zhou et al. (2016). Cai et al. (2017) propose an analytical solution for the reliability analysis of slope stability in the presence of spatially variable shear strength parameters.

This paper investigates the effects of non-homogeneous vertical soil profiles on the required armour layer thickness. For this purpose, an infinite slope model was modified to account for ship-induced drawdowns, resulting excess pore pressures and the armour layer. Within the limitations of the infinite slope assumptions, the effects of a spatially variable friction angle and hydraulic conductivity are investigated by means of a 1D random field. The introduction of spatially variable soil parameters allows to account for spatial variability explicitly and, thereby, to assess the level of safety obtained with current design approaches. In a parameter study that covers local and spatial variability, a deterministic benchmark solution and the results of the probabilistic random field analyses are compared.

The paper is organised as follows: The first section introduces the infinite slope model, briefly touching on aspects such as the pore pressure determination, the random field generation and the parameter combinations used for the analysis. In the subsequent section, the results of the random field analyses are presented with regard to the required thickness of the armour stone layer and compared to deterministic benchmark solutions. The probability of slope failure and, thus, the current level of safety is outlined in Section 4. In Section 5 methodology and findings are discussed. The paper closes with recommendations regarding site exploration, choice of characteristic values and an outlook for future research.

2 Basic formulation and methods

2.1 Design equations of the infinite slope model

One of the oldest and simplest models for slope stability analysis is the 1D infinite slope model, which models slopes extending a long distance up and down the slope. Assuming identical conditions on any vertical section and a failure plane parallel to the surface of the slope, the model assesses the limit equilibrium of a single vertical "column" of the slope analytically. The equations for the 1D infinite slope model outlined herein follow the formulation of Zhou et al. (2016), which have been modified to account for the drawdown-induced excess pore pressure and the armour layer stabilizing the embankment.

It is assumed that the shear stress $\tau\,(\mathbf{v}, y)$ and the shear strength $\bar{\tau}(\mathbf{v}, y)$ are constant at any given depth y in the downslope direction, where $\mathbf{v}$ represents stochastic variables that are included in the calculation. The spatial variability of the soil parameters is modelled as a 1D random process. Considering an infinite slope, the failure criterion for an arbitrary plane is that $\tau\,(\mathbf{v}, y)$ on the plane exceeds $\bar{\tau}(\mathbf{v}, y)$ on the plane. Following the notation commonly used in reliability engineering, the failure criterion is expressed as the limit state function g as follows:

$$g(\mathbf{v}, y) = \bar{\tau}(\mathbf{v}, y) - \tau\,(\mathbf{v}, y) \qquad (y \in [0, y^*]) \tag{1}$$

where y^* is the thickness of the layer under consideration.

The shear stress τ is caused by the effective vertical overburden stress σ_v' which results from the self-weight of the soil mass and the pore water. With the slope inclination α it can be written as:

$$\tau(\mathbf{v}, y) = \sigma_v'\,(y) \sin \alpha \cos \alpha \tag{2}$$

where σ_v' without a revetment is determined by eq. (3) and with a revetment by eq. (4):

$$\sigma_v'\,(y) = \gamma' y \tag{3}$$

$$\sigma_v'\,(y) = \gamma' y + [(\gamma_r - \gamma_w) \cdot (1 - n_r)] \cdot \left(\frac{d_D}{\cos \alpha}\right) \tag{4}$$

Eq. (3) and eq. (4) include the soil buoyant unit weight γ', the saturated unit weight of the armour stones γ_r, the unit weight of water γ_w, the porosity of the armour stone layer n_r and the thickness of the armour stone layer d_D.

The shear strength $\bar{\tau}(\mathbf{v}, y)$ is described by the Mohr-Coulomb criterion, which features the effective normal stress acting on the soil skeleton σ_n, the effective friction angle ϕ' and the effective cohesion c', and reads as follows:

$$\bar{\tau}(\mathbf{v}, y) = \sigma'_n\,(y)\tan \phi'(y) + c' \tag{5}$$

In the case of a vessel passage, σ'_n is reduced by the excess pore pressure Δp.

$$\sigma'_n (y) = \sigma'_v (y) \cos^2 \alpha - \Delta p \tag{6}$$

If the soil has a permanent effective cohesion under water greater than Δp, the local slope stability of permeable revetments can be assumed without further verification (GBB, 2010). Thus, the subsequently presented investigation only considers non-cohesive materials ($c'= 0$ kN/m²). Moreover, to ensure that the infinite slope assumptions are not violated, the investigations focus on the submerged part of the slope (GBB, 2010).

2.2 Determination of excess pore pressures

In the case of the investigated ship-induced drawdown, the difference between the pore pressure from hydrostatic conditions in the canal and the current pore pressure in the soil's voids is termed excess pore pressure. It arises when the soil cannot drain fast enough in response to the rapid load change. As a result, a difference between the pore pressure in the embankment and the hydrostatic pressure at the water/soil interface develops and the gradient changes (see Figure 2).
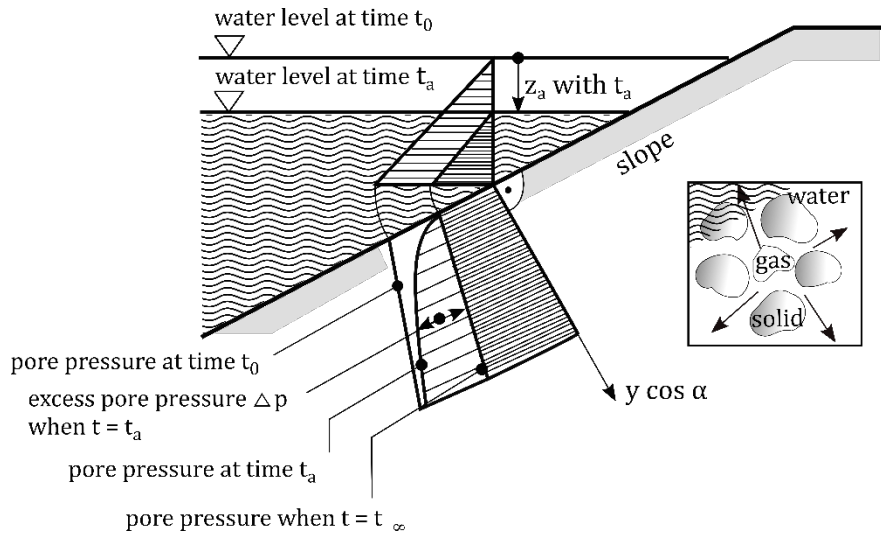
Figure 2: Hydrostatic pore water pressure and excess pore water pressure during ship-induced drawdown. Adapted from GBB (2010).

For the purpose of the presented analyses, we consider a porous, deformable soil skeleton saturated with a compressible fluid, i. e. a water-gas-mixture (Madsen, 1978). The problem of coupled interstitial flow and deformation is a time-dependent process. However, as found by Köhler (1989) a quasi-static behaviour can be assumed. The unknown fields are then the displacement $\boldsymbol{u}$ of the solid and the pore-fluid pressure p over the time t.

The governing equation system is solved using several constitutive relationships. As shown in eq. (7), the tensor of effective stresses is related to the displacement field:

$$\boldsymbol{\sigma'} = \boldsymbol{C} : \boldsymbol{\epsilon} \tag{7}$$

where $\boldsymbol{C}$ is a fourth-order tensor of the material stiffness and $\boldsymbol{\epsilon}$ is the strain tensor. Here, an isotropic linear elastic stress–strain relationship is considered. Moreover, for simplicity, we adopt a small-strain assumption:

$$\boldsymbol{\epsilon} = \frac{1}{2} (\nabla \boldsymbol{u} + \nabla \boldsymbol{u}^T) \tag{8}$$

The governing balance equations for coupled flow deformation can be written as:

$$\nabla \cdot \boldsymbol{\sigma'} + \nabla p + \rho_m \boldsymbol{g} = 0 \tag{9}$$

$$\frac{\partial \rho_m}{\partial t} + \nabla \cdot \frac{\partial \mathbf{u}}{\partial t} + \nabla \cdot \boldsymbol{q} = 0 \tag{10}$$

where $\boldsymbol{\sigma}'$ is the effective stress, ρ_m is the density of the porous medium and fluid, $\boldsymbol{g}$ is the gravity vector and $\boldsymbol{q}$ is the seepage velocity vector determined by Darcy's law with $\boldsymbol{k}$ as the tensor of the hydraulic conductivity. The change of ρ_m over time is a function of the effective bulk modulus of the pore fluid K', the porosity of the solid material n_s and the pore pressure:

$$\frac{\partial \rho_m}{\partial t} = \frac{n_s}{K'}\frac{\partial p}{\partial t} \tag{11}$$

The density of the porous medium and fluid ρ_m is the mixture density of the solid ρ_s, the water ρ_w and the gas ρ_g and the degree of saturation S which is the percentage of the void space filled with water (Montenegro, 2016). The lower S, the more gas the water-gas mixture contains and, thus, the more compressible the mixture.

$$\rho_m = n_s S \rho_w + (1-S)\rho_g + (1-n_s)\rho_s \tag{12}$$

The pore-fluid compressibility (inverse of K') is expressed as follows:

$$\frac{1}{K'} = \frac{S}{K_w} + \frac{(1-S)}{(p_g + p_a)} \tag{12}$$

where K_w is the bulk modulus of water, p_g is the gas pressure and p_a is the atmospheric pressure. Since an equilibrium between enclosed gas phase and surrounding water phase is assumed, $p_g = \overline{p_w}$ where $\overline{p_w}$ is the mean of the hydrostatic pore pressure over depth.

As initial conditions we assume a field of zero displacements and hydrostatic pore pressures. As boundary conditions zero displacement and zero flow are prescribed at the bottom of the soil column. At the top of the soil column the pressure resulting from the drawdown and zero total traction are stipulated. Detailed information on initial and boundary conditions are given in the Appendix.

In the case of the presented study, a one-dimensional (1D) flow-deformation finite element (FE) model is employed to evaluate the drawdown-induced excess pore pressure over depth. The validation of the model can be found in Montenegro (2016). Admittedly, the flow caused by a rapid drawdown in a homogeneous slope is at least a two-dimensional (2D) problem. However, as demonstrated by Ewers et al. (2017), who compared the development of excess pore pressures in soils of different compressibility properties in a 1D finite element column model to that of a 2D finite element slope model, 1D computations can yield an acceptable approximation of the 2D slope problem.

2.3 Random field generation

The spatial variability of ϕ' and k is modelled by means of two independent random fields. Numerous methods have been proposed for the generation of random fields, such as the covariance matrix decomposition (CMD) method (Davis, 1987; Clifton and Neuman, 1982), the moving average (MA) method (Gersch and Yonemoto, 1977), the turning bands method (TBM) (Matheron, 1973), the fast Fourier transform (FFT) method (Cooley and Tukey, 1965) and the local average subdivision (LAS) method (Fenton and Vanmarcke, 1990).

This work is restricted to stationary random fields where the covariance between two points depends solely on their distance. The random fields are generated by the CMD method with a Cholesky decomposition. Firstly, a standard normal distribution is generated, in which the spatial variation of the standard values is incorporated by means of a correlation function with a scale of fluctuation $\theta_{k,\phi'}$. An exponential correlation function adopted from (Griffiths et al., 2011) is applied:

$$\rho(\Delta y|\theta) = \exp\left(-\frac{2|\Delta y|}{\theta}\right) \tag{13}$$

In simple terms, $\theta_{k,\phi'}$ describes the maximum distance over which values are spatially correlated. This means that values within this range are correlated, albeit decreasingly so with increasing distance. The mathematical definition of the scale of fluctuation can be found in, e. g., Vanmarcke (2010).

The standard normal field is next transformed to the appropriate distribution based on the mean μ and coefficient of variation (cov) of the variable being modelled. A lognormal distribution of the random variables will ensure the variables are bounded by $\phi' > 0\,°$ and $k > 0$ m/s. The lognormal distribution is a common choice in geotechnical engineering as it offers the advantage of simplicity. The parameters are derived by a simple nonlinear transformation of the Gaussian distribution, e. g. Griffiths and Fenton (2007). Figure 3 illustrates the random field parameters and the corresponding calculation models schematically with regard to the infinite slope.
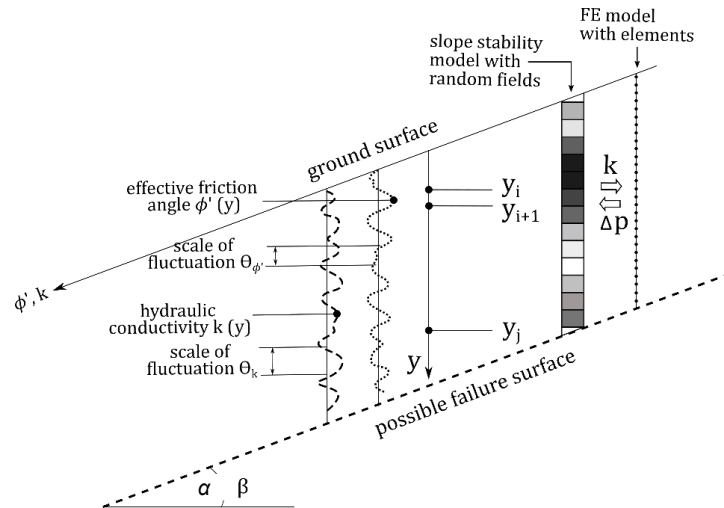

Figure 3: Schematic diagram of the random field method applied to an infinite slope. Random fields of k and ϕ' are generated; k is mapped to the FE model to determine the excess pore pressures Δp which are re-assigned to the infinite slope model by linear interpolation.

2.4 Revetment design in the presence of random fields

As a result of a fast drawdown, the limit state function g (see eq. (1)) reaches a minimum g_{min} at a certain depth, which is also referred to as the critical depth d_{crit}. If $g_{min} < 0$, it may result in a local slope sliding failure. A revetment whose capacity is governed by the layer thickness and the weight of the armour stones can prevent such failures as it leads to an increase in effective stress. The required armour layer thickness d_D is derived from the infinite slope equations at g_{min}:

$$d_D \geq \frac{g_{min}(v)}{(\sin\beta - \tan\phi'\cos\beta)\cdot[(\gamma_r - \gamma_w)\cdot(1-n_r)]} \tag{14}$$

For the stability analysis using the random field approach, 50 000 Monte Carlo (MC) simulations are run to obtain a range of possible outcomes. With each simulation, a random field with the same target mean and standard deviation, but with a different spatial distribution of soil properties within the 1D column is generated. Under the assumption that failure of any plane in the slope causes a local failure, g_{min} is recorded after each simulation and compared to the following scheme:

$$I = \begin{array}{ll} \text{stable (0),} & g_{min}(v) \geq 0 \\ \text{unstable (1),} & g_{min}(v) < 0 \end{array} \tag{15}$$

where I is an indicator function. The probability of a slope failure p_f then results from the number of failures relative to the overall number of simulations N.

$$p_f = P[I = 1] \approx \frac{1}{N}\sum_{i=1}^{N} I_i \tag{16}$$

Reviewing eq. (2) and eq. (4), it becomes clear that the application of the armour stones will increase the vertical overburden load and, thereby, stress and strength. However, whereas the shear stress τ rises proportionally with increasing overburden load, the shear strength $\bar{\tau}$ rises non-proportionally due to the multiplication of σ'_n by $\tan \phi'$, see eq. (5). The resulting difference between stress and strength requires more armour stones after initial equilibrium. Thus, the required armour stone layer thickness has to be found by means of iterative analyses.

Considering an example design case, where the initial calculation is conducted without a revetment, the first guess of the required armour layer thickness can be obtained by an evaluation of eq. (14). However, as outlined above, the application of this newly calculated armour layer thickness may result in $g_{min} < 0$, since eq. (14) only accounts for the load situation (g_{min}) at the time of initial calculation. An additional calculation is thus required to assess whether the currently assumed armour layer thickness is sufficient to ensure local slope stability. If the calculations indicate that more armour stones are necessary to fulfil equilibrium, a third, fourth, and so on, evaluation of eq. (14) with the armour layer thickness determined in each step is required to verify that $g_{min} \geq 0$.

The complete workflow of the calculations is illustrated in Figure 4. First, a random field of 500 slices is generated. Based on their coordinates the spatially variable material properties are mapped to the finite element model with 1000 elements to determine the resulting excess pore pressures. The time discretisation of the FE model amounts to 0.05 x drawdown time t_a. The excess pore pressures are subsequently assigned to the slope stability model by linear interpolation. The required armour layer thickness is then derived from the slope stability model calculations, which use material strength and excess pore pressures as input. The two-step approach with separate excess pore pressure and slope stability models is required to increase the calculation efficiency. The excess pore pressure model requires a significantly higher resolution than the stability analysis. Subsequently, 50 000 Monte-Carlo simulations are conducted to determine the required armour layer thickness. In each simulation, new random fields are created for the ground properties based on the probability density functions and characterised by the same statistics (μ, cov, θ). Each time the inner iteration loop is completed, the armour layer thickness is increased until $g_{min} \geq 0$ is reached.

```
Layer thickness d_D = 0
├─ While P(g_min < 0)
│       MC simulations
│     ├─ For i=1:50 000
│             Random field generation
│             with slices=500

│             FE excess pore pressure calculation
│             with elements=1000

│             Stability calculation to obtain g_min
│             with slices=500
│     └─ End
│         Increase d_D
└─ End
```
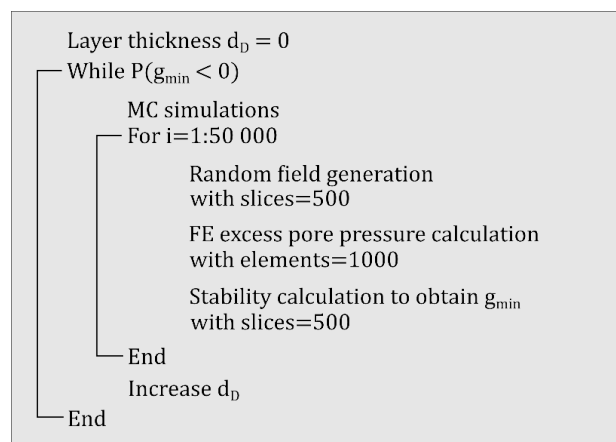
Figure 4: Calculation procedure to determine the layer thickness with a random field

The above described iteration procedure where the armour layer thickness is increased repeatedly is equally required for the benchmark and probabilistic analyses. Since Sections 3.1 - 3.3 focus on the comparison between benchmark and probabilistic analyses, the results after the first iteration are presented. A brief study, which is not part of this paper, shows that the first iteration provides valid results for a comparison. Only in Section 4 the iterative analysis which yields the armour layer thickness required for construction is used to evaluate p_f.

2.5 Parameter combinations

The soil types and drawdown combinations are selected based on the existing German design standards (MAR, 2008; EAU, 2012). For the purpose of illustration, a permeable sand (SW) and a silty sand (SU) are investigated. While the hydraulic conductivity of the silty sand is smaller by a factor of 10 than for the sand, the range of friction angles is the same for both soil types. Moreover, the silty sand is characterised by a smaller effective unit weight γ'. The cov are based on the parameter range provided by MAR (2008) and EAU (2012). The elastic properties, i. e. unconstrained stiffness

modulus E_S and K', are assumed to be constant and, thus, independent of the spatially varying parameters. In the presented investigations $S = 85$ %, $E_S = 30$ MPa and $n_s = 0.45$ are specified as conservative estimates.

The selected drawdowns are worst case assumptions regarding a vessel passage in a standardised rectangular trapezoidal profile of a waterway cross-section (MAR, 2008). No distinction is made between bow and stern drawdown. From the load combinations available in MAR (2008) the most unfavourable are chosen based on a small parametric study. Combining load combinations and soil types, the four representative case studies summarised in Table 1 are investigated.

Table 1: Combinations of loads and soil types with their physical properties.

Soil type	Mean effective friction angle ϕ'	cov	Mean hydraulic conductivity k	cov	Effective unit weight γ'	Draw-down time t_a	Draw-down height z_a
--	°	--	m/s	--	kN/m³	s	m
Widely graded sand (SW1)	35.0	0.01 - 0.04	5.5E-05	0.05 - 0.50	11.5	4.5	0.63
Widely graded sand (SW2)	35.0	0.01 - 0.04	5.5E-05	0.05 - 0.50	11.5	27.6	0.83
Silty sand (SU1)	35.0	0.01 - 0.04	5.5E-06	0.05 - 0.50	9.5	4.5	0.63
Silty sand (SU2)	35.0	0.01 - 0.04	5.5E-06	0.05 - 0.50	9.5	27.6	0.83

The model variables k and ϕ' are defined as follows: the target mean value for the random field is constant, while the variation of the properties relative to the mean is governed by the cov. For the deterministic benchmark solution, a range of ϕ' and k are considered, since the GBB (2010) does not provide specific guidance for the choice of characteristic values. The lower bound is taken as the 5 % quantile of the distribution in accordance with the characteristic value in the case of a local failure mechanism (DIN1997-1:2014-03). The upper bound of the deterministic benchmark solution is the mean, which is an optimistic assumption for failure mechanisms where spatial averaging occurs (Vanmarcke, 1977). Figure 5 illustrates the approach for two distributions with different standard deviations. Henceforth, results that consider the spatial variability are denoted by "rf", whereas the corresponding benchmark results are indicated by the abbreviation "bm".
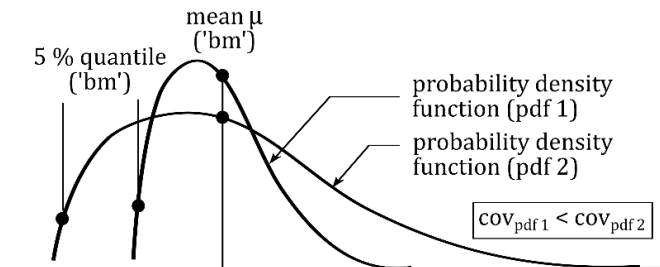

Figure 5: Parameter definition to compare the random field analyses to the benchmark solution. The 5 5 quantile and the mean marked by the black circles indicate the upper and lower limits of the benchmark solution

3 Results

3.1 Influence of a non-homogeneous friction angle

Firstly, to investigate the influence of a non-homogeneous ϕ', k is kept constant at its mean value, while $cov_{\phi'}$ and $\theta_{\phi'}$ are varied. The results are presented in Figure 6. It can be observed that for the deterministic "bm" and probabilistic "rf" solutions, the required armour layer thickness is a function of $cov_{\phi'}$. The results indicate that with an increasing $cov_{\phi'}$ the deterministic 5 % "bm" results require more or equal armour stones than the "rf" results, whereas deterministic mean "bm" calculations require less armour stones. Increasing $\theta_{\phi'}$ values do not affect the required armour layer thickness significantly. However, for soils of lower permeability, the 5 % benchmark solution is not conservative for small $\theta_{\phi'}$. In the case of $\theta_{\phi'}$, the combination of low ϕ' and low k near the surface is crucial for the embankment stability. Close to the

surface, the excess pore pressure rises while the superimposed load of the soil and the shear strength remain low resulting in larger armour layer thicknesses.
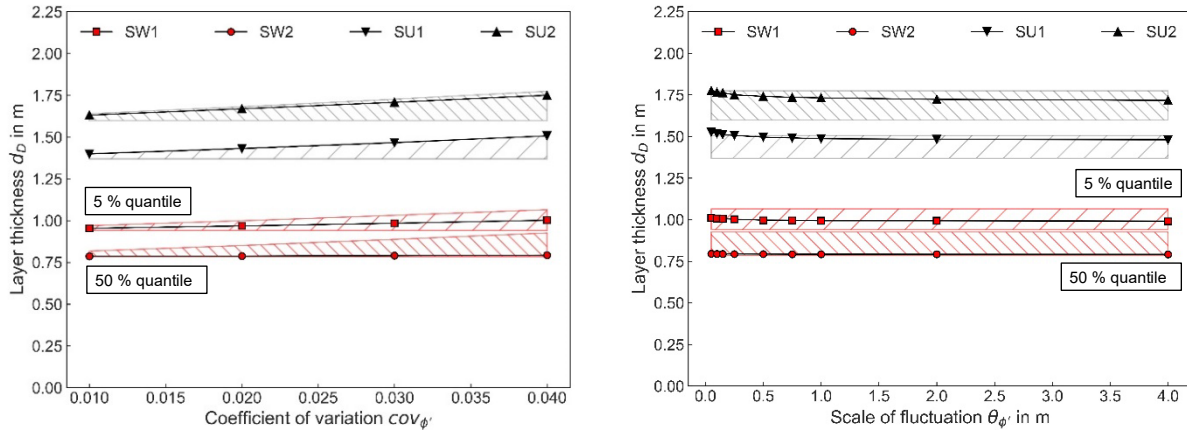
(a) Required layer thickness as a function of $cov_{\phi'}$ with $\theta_{\phi'} = 0.25$ m

(b) Required layer thickness as a function of $\theta_{\phi'}$ with $cov_{\phi'} = 0.04$

Figure 6: Influence of a non-homogeneous effective friction angle on armour layer thickness (first iteration without initial overburden load). The hatched areas indicate the deterministic benchmark solutions obtained with the 5 % and 50 % quantiles. The lines with markers depict the 95 % quantiles obtained from the uncertainty analysis with random ϕ'.

In addition, it can be observed that the layer thickness required for the SW cases is governed by the combination of small t_a at moderate z_a, whereas the layer thickness of the SU cases is governed by the combination of large t_a at large z_a. This observation can be explained by the time required to reach a quasi-stationary state, which means that temporal variations of the excess pore pressure are much smaller than spatial variations. In soils of smaller hydraulic conductivity, it takes longer to reach this quasi-stationary state, while in permeable soils the quasi-stationary state is reached faster. This results in larger excess pore pressures and armour layer thicknesses for large t_a in the case of less permeable materials, whereas in the case of permeable materials a larger z_a/t_a ratio causes larger excess pore pressures and requires larger armour layer thicknesses.

With regard to the revetment design, the results of the sandy material indicate that the choice of the 5 % quantile of ϕ' as the characteristic value may overestimate the required armour layer thickness. In contrast, for less permeable soils, the results indicate that the choice of the 5 % quantile of ϕ' as the characteristic value may ensure engineering safety although it is not a strictly conservative solution. Furthermore, the analyses indicate that the combination of k and the drawdown parameters affect the design more strongly than the variability of ϕ'.

3.2 Influence of a non-homogeneous hydraulic conductivity

In this section the influence of a non-homogeneous k is investigated with a constant ϕ' and a varying cov_k and θ_k. Figure 7 (a) shows that an increasing variance of k does not affect the armour layer thickness notably. The increasing cov_k in the "rf" cases demands a similar layer thickness as the 5 % "bm" results. In contrast, Figure 7 (b) shows that small θ_k values yield slightly smaller layer thicknesses than the 5 % "bm" solutions. A thin "layering" reduces the maximum excess pore pressure and thus the required armour layer thickness. For $\theta_k \to 0$, k reaches the harmonic mean, which is slightly smaller than the arithmetic mean of the probability density function, but larger than the 5 % "bm". The harmonic mean of the hydraulic conductivity k_{eff} is determined from the sum of n individual random field slices L_i over their hydraulic conductivities k_{si} compared to the total layer thickness, see eq. (17). For $\theta_k \to \infty$ the "rf" results approach the 5 % "bm". Comparing the two drawdowns considered, these observations are more prominent for the larger drawdown height at low(er) velocity (SW2, SU2) than for a small(er) drawdown height at great(er) velocity (SW1, SU1).

$$k_{\text{eff}} = \frac{\sum_{i=1}^{n} L_i}{\sum_{i=1}^{n} \frac{L_i}{k_{si}}} \tag{17}$$
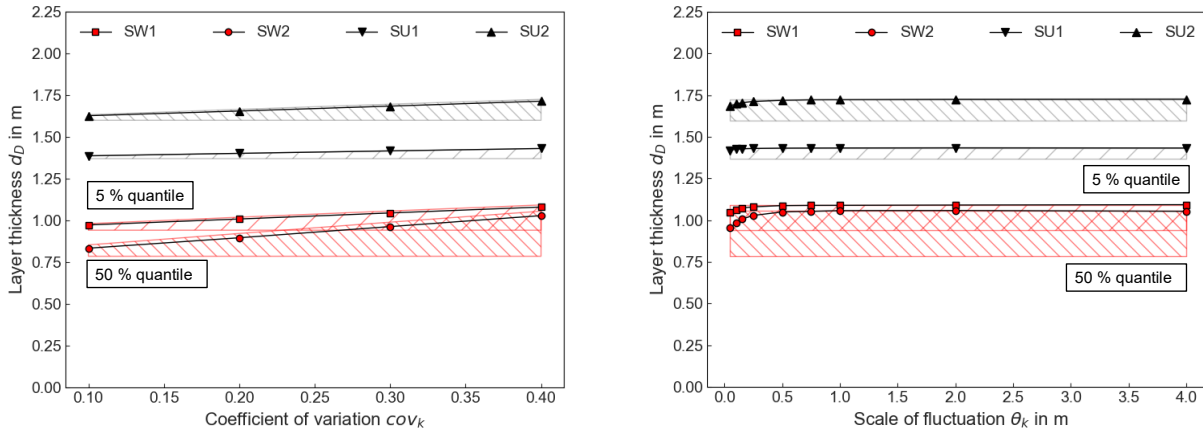
(a) Required layer thickness as a function of cov_k with $\theta_k = 0.25$ m

(b) Required layer thickness as a function of θ_k with $cov_k = 0.4$

Figure 7: Influence of a non-homogeneous hydraulic conductivity k on armour layer thickness (first iteration). The hatched areas indicate the deterministic benchmark solutions, whereas the markers depict the 95% quantiles obtained from the uncertainty analysis with random k.

In the context of a revetment design, the results indicate a significant influence of the spatial variability of k on the required armour layer thickness. Especially soils of higher permeability exhibit a noteworthy sensitivity to fluctuating k values at different θ_k. Figure 7 indicates that the 5 % quantile of k may not be as conservative as assumed. In all of the four design cases, the "rf" armour layer thicknesses just meet the layer thicknesses determined in the 5 % "bm" solutions. Furthermore, the results imply that in any case the least permeable areas govern the design. Particularly, if these areas are greater than approximately 0.25 m, they will act as a seal and the excess pore pressure will increase to the 5 % "bm" solution; hence, more armour stones will be required.

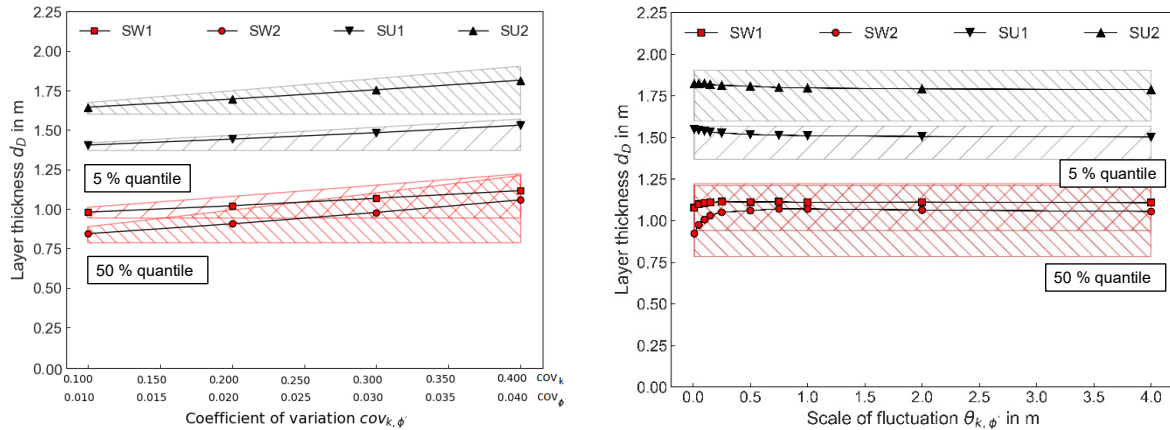## 3.3 Influence of a non-homogeneous friction angle and hydraulic conductivity

Finally, the combination of a non-homogeneous friction angle and hydraulic conductivity is investigated, assuming no correlation between ϕ' and k. For simplicity, $cov_{\phi'}$ and cov_k change synchronously, which may not be fully consistent with the engineering situation. However, we consider that when less information is available in general the uncertainty and, thus, the variability of both k and ϕ' increase simultaneously.

Figure 8 illustrates that the mean "bm" calculations underestimate the required armour layer thickness. In contrast, the 5 % "bm" cases overestimate the required armour layer thickness compared to the "rf" analyses with different $\theta_{k,\phi'}$ and $cov_{k,\phi'}$ values. With increasing $cov_{k,\phi'}$, the difference between the "rf" and "bm" cases increases. Consequently, the characteristic values of ϕ' and k should be considered as a function of $cov_{k,\phi'}$.

Noteworthy is the different behaviour of the SW and SU cases with regard to an increasing $\theta_{k,\phi'}$ (see Figure 8 (b)). In both SW cases, the required armour layer thickness initially rises until a maximum is reached, whereas the SU cases do not show a pronounced effect on the armour layer thickness with increasing $\theta_{k,\phi'}$. This behaviour may be explained by the larger variability of the excess pore pressure profiles in permeable soils (see Section 3.4). It is assumed that with smaller hydraulic conductivity the influence of the spatial variability on the excess pore pressures decreases.

Based on the four case studies, a worst case correlation length that requires the attention during design can be established. The examples indicate that a correlation length that ranges in the area of the critical depth affects the required armour layer thickness most. For the SU cases d_{crit} ranges between 0.20 m and 0.50 m, whereas the SW cases are characterised by a greater d_{crit} of 0.40 m to 0.60 m. In the SW cases, the 5 % "bm" solution gives significantly larger armour layer thicknesses than the probabilistic approach for $\theta_{k,\phi'}$ smaller than d_{crit}. In contrast, in the SU cases, the probabilistically determined required armour layer thickness decreases slightly for $\theta_{k,\phi'}$ greater than d_{crit}. Yet, the analyses show that

for the combination of ϕ' and k, all investigated benchmark studies ensure engineering safety although on different levels of safety.

(a) Required layer thickness as a function of $cov_{k,\phi'}$ with $\theta_{k,\phi'} = 0.25$ m

(b) Required layer thickness as a function of $\theta_{k,\phi'}$ with $cov_k = 0.4$ and $cov_{\phi'} = 0.04$

Figure 8: Influence of a non-homogeneous hydraulic conductivity k and effective friction angle ϕ' on armour layer thickness (first iteration). The hatched areas indicate the deterministic benchmark solutions, whereas the markers depict the 95 % quantiles obtained from the uncertainty analysis with random k and ϕ'.

3.4 Summary of influence of heterogeneous ϕ' and k on the embankment stability

The consideration of vertically heterogeneous ϕ' and k leads to two competing mechanisms. While areas of larger ϕ' increase the stability of the embankment and thus require less armour stones, the presence of smaller k leads to larger excess pore pressures and thereby to a thicker required armour stone layer. Figure 9 displays the stress, strength, excess pore pressure and limit state profiles over depth with the corresponding random fields for a best-case and a worst-case simulation of the sand and the silty sand. Naturally, larger excess pore pressures occur in the presence of low values of k. A worst case scenario is characterised by a low k (and a low ϕ') close to the surface; conversely, a higher k close to the surface leads to smaller excess pore pressures in the area close to the surface.

Considering once more eq. (14), the required armour layer thickness is determined by g_{min}. In particular, when geotechnical units of low k and a thickness greater 0.25 m are located close to the surface, large excess pore pressures can occur. As a result of the excess pore pressures the effective shear strength decreases, which, in the case of a low overburden weight of the soil close to the surface, can only be compensated by larger ϕ'. In areas of larger ϕ', it is thus more likely that the maximum excess pore pressure can be compensated by the material strength. As a consequence, for revetment design, subsoil investigations and subsequent stability analyses should pay special attention to the variability of k and ϕ', in particular close to the surface.

4 Probability of slope failure

The design or assessment of a revetment may target a specific reliability. The reliability of the revetment is a function of the drawdown, the slope inclination, the soil parameters and the armour layer thickness. Since drawdown, geometry and soil parameters are commonly defined on the basis of available field information, the representative parameter sets of case studies SW2 and SU2 are selected to investigate the reliability as a function of the armour layer thickness. Each case study is investigated the following combinations:

- $\theta_{k,\phi'} = 0.50$ m, $\theta_{k,\phi'} = 1.00$ m,
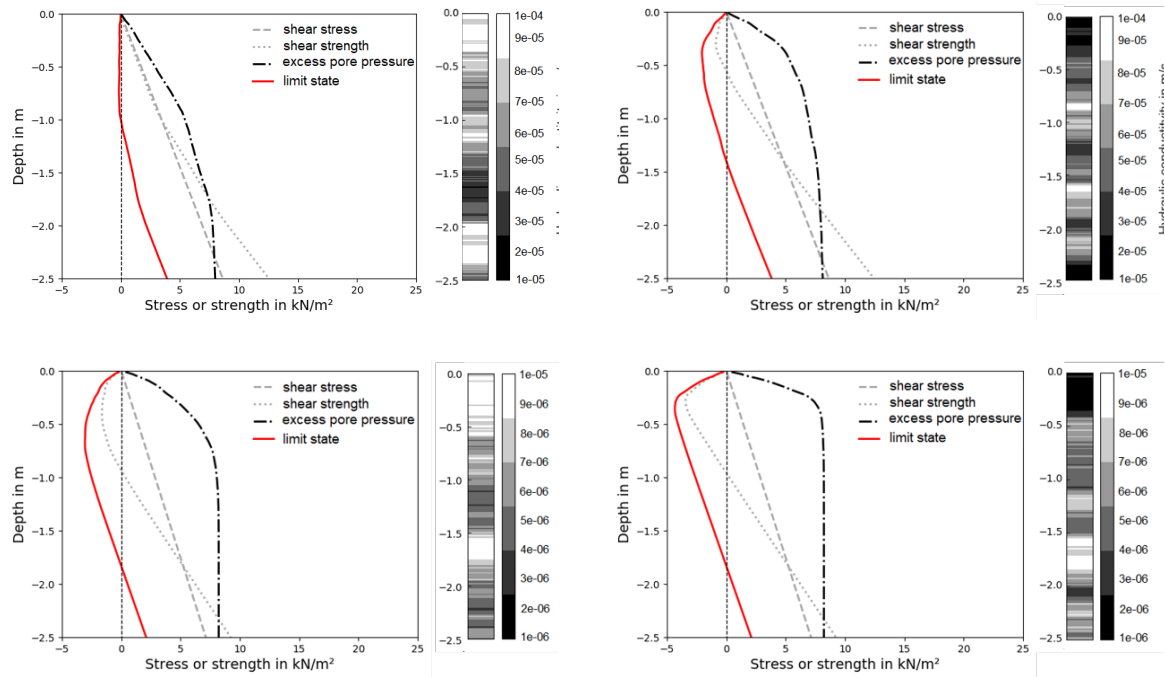- $cov_{k,\phi'} = 0.20/0.02$, $cov_{k,\phi'} = 0.40/0.04$.

Figure 9: Stress, strength, excess pore pressure and limit state proles with the corresponding random field for maximum (left) and minimum (right) limit state g out of 50 000 MC simulations for SW2 (top) and SU2 (bottom) with cov_k = 0.4 and θ_k = 0.5 m.

As shown in Figure 10, the probability of failure p_f decreases with increasing layer thickness rather rapidly after a certain threshold value has been reached. The larger the $\text{cov}_{k,\phi'}$, the larger the p_f, whereas $\theta_{k,\phi'}$ does not significantly influence p_f although this may be due to the investigated $\theta_{k,\phi'}$ which are smaller than d_{crit}. For larger $\text{cov}_{k,\phi'}$ the p_f of the two investigated $\theta_{k,\phi'}$ are concordant.

(a) Sand (SW2)

(b) Silty sand (SU2)
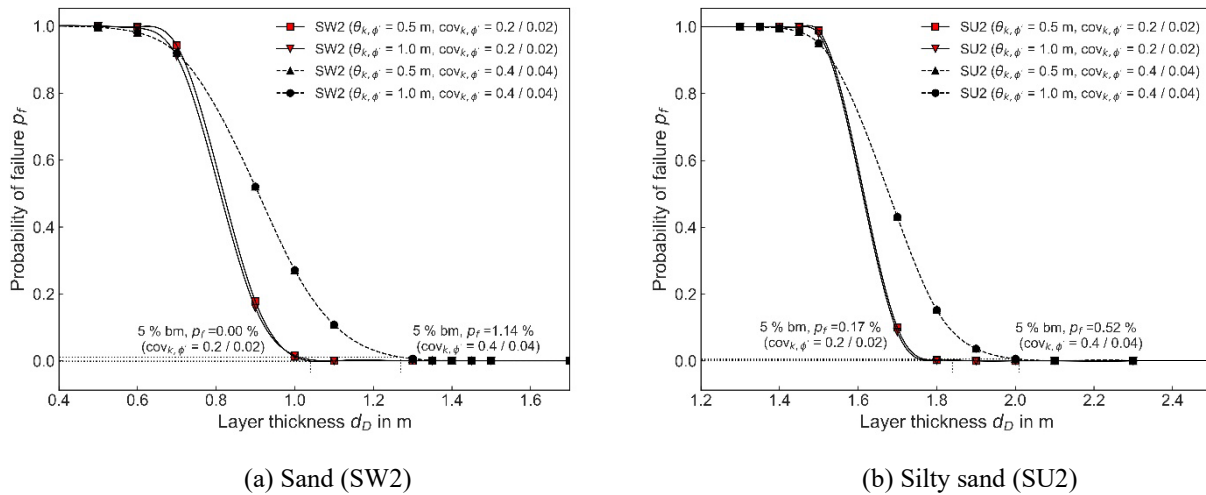
Figure 10: Probability of failure for different materials and variability parameters. The highlighted values indicate the probabilities of failure at the time of model convergence.

The obtained probabilities of failure highlight the importance of an iterative analysis (see Section 2.4) or the use of probability charts when using the infinite slope model for a revetment design. In the case of SU2, for instance, the layer thickness obtained after one iteration (see Section 3.3) yields p_f = 80 % for $\text{cov}_{k,\phi'}$ = 0.20 / 0.02 and p_f = 40 % for $\text{cov}_{k,\phi'}$ = 0.40 / 0.04. Since the probability graphs of $\text{cov}_{k,\phi'}$ = 0.20 / 0.02 are characterised by a steeper gradient in the area of interest, smaller iteration steps than for larger $\text{cov}_{k,\phi'}$ are required.

According to JCSS (2001), a target reliability of $\beta = 3.1$ ($p_f = 1E\text{-}03$) may be acceptable for ultimate limit states leading to minor consequences in the case of a failure while characterised by high costs for safety measures. The armour layer thicknesses, which are determined after several iterations with increasing layer thicknesses using the 5 % "bm" values, reach $p_f \approx 0.00$ % - 1.14 % and thus do not meet the target reliability. In the cases studied, the inaccuracy of the deterministic analyses increases with the soil's variability. Furthermore, the inaccuracy is greater for permeable soils than for less permeable soils. If the current level of safety is satisfactory, the choice of limit state condition and target reliability should be discussed. Otherwise, the current choice of characteristic values has to be to be revised.

5   Discussion

The presented investigations illustrate the effects of a spatially variable friction angle and hydraulic conductivity on the revetment design. The applied methodology is not suitable for direct comparison with the existing German standard, since the excess pore pressures determined by an FE model based on Biot's approach (Biot, 1956) are different to the excess pore pressures calculated using the analytical approximation defined in the GBB (2010). However, the parameter study indicates a strong model sensitivity to the excess pore pressure profiles, which once more emphasises the significance of an accurate method to describe the development of the pore water pressures.

In addition, the current investigations do not take a toe support into account, which significantly reduces the required armour layer thickness due to the activation of additional supporting shear stresses. Such a simplification is justifiable with respect to the aim of these investigations. A toe support should not alter the observed mechanisms. This, however, results in rather large layer thicknesses for the current investigations. In general, it can be assumed that the construction of a toe support reduces the required armour layer thickness by 0.60 m to 0.90 m.

The analyses do not account for correlation between different soil parameters. In the case of the investigated parameters the correlation is slightly negative (Arnold and Hicks, 2011; Vardon et al., 2016). A zone that is characterised by small ϕ' is more likely to be associated with high k and vice versa. In this case, a negative correlation would tend to reduce best- and worst-case scenarios. However, if considering a correlation of the matrix stiffness K_s as well, competing mechanisms affecting the required armour layer thickness may be observable. While a correlation of ϕ' and k mainly governs the resistance, a correlation of K_s, k and the material porosity n influences the excess pore pressure development. Hence, more research is required.

Despite these limitations, the results demonstrate that the level of safety obtained with the deterministic (or semi-probabilistic) design approach depends strongly on the choice of the characteristic values. The choice of characteristic values, in turn, is a function of not only the absolute values, but also the variance and the scale of fluctuation of the respective ground properties. In the case of ϕ', the 5 % quantile may overestimate the required armour layer thickness for permeable soils, while a value between the lower third and a conservative mean may be a suitable choice. In contrast, for less permeable soils, the 5 % quantile of ϕ' as the characteristic value may ensure engineering safety. In the case of k, the 5 % quantiles may lead to slightly unconservative designs for $\theta_k > d_{crit}$. For a combination of ϕ' and k the 5 % quantiles may overestimate, and the mean values may underestimate, the required armour layer thickness if uncorrelated parameters are assumed. Depending on $cov_{k,\phi'}$ and $\theta_{k,\phi'}$, the "rf" analyses require between 10 cm to 30 cm less armour stones than the 5 % "bm" solutions.

Moreover, GBB (2010) states that the combination of ϕ' and k requiring the highest weight per unit area determines the revetment dimensions. However, only geotechnical units greater than 1 m are considered for the design. Subsequently, a homogeneous slope is assumed for stability analysis. The results, however, suggest that less permeable zones greater than 0.25 m thickness located close to the surface govern the excess pore pressure and the required armour layer thickness. Especially in the near-surface area, soil units smaller than 1.0 m should therefore be considered for design.

6 Conclusions

The investigations show that the level of safety obtained with the deterministic design approach depends strongly on the choice of the characteristic values. Particularly, the choice of the characteristic value of the hydraulic conductivity determines the reliability of the design. The best estimates of the characteristic values are a function of ϕ', k, $\text{cov}_{k,\phi'}$ and $\theta_{k,\phi'}$. A "worst case" $\theta_{k,\phi'}$ is identified.

As a consequence, for revetment design, subsoil investigations and subsequent stability analyses should pay special attention to the variability of k and ϕ', in particular close to the surface. To obtain a reliable design, the characteristic value for k should be selected as a value at the lower end of the explored parameter range, whereas the characteristic value of ϕ' may be selected depending on the soil type as a value between the 5 % quantile and a conservative mean. As the worst-case correlation length is most critical in the range of the critical depth, it is recommended that the selection of characteristic values should be based on the least permeable zone located between zero depth and the critical depth.

Further investigations regarding the comparability of the target reliabilities available in current probabilistic design codes and the level of safety of the current design are required. Moreover, the investigations should consider the correlation between the soil parameters and the spatial variability of the elastic soil properties. Finally, it is emphasised that further investigations of the probabilistic distribution of the loads are necessary in order to conduct a fully probabilistic revetment design.

Acknowledgements

Author contributions (CRediT)

JS[1]: Conceptualization, Formal Analysis, Validation, Visualization, Writing – original draft. APvdE[2]: Conceptualization, Writing – review & editing. HM[3]: Methodology & Validation of coupled flow-deformation finite element model, Writing – review & editing. MAH[4]: Supervision, Writing – review & editing.

Notation

Name	Symbol	Unit
Slope inclination	α	$°$
Reliability index	β	
Soil buoyant unit weight	γ'	kN/m^3
Saturated unit weight of the armour stones	γ_r	kN/m^3
Unit weight of water	γ_w	kN/m^3
Strain tensor	ϵ	
Scale of fluctuation	θ	m
Mean	μ	
Correlation function	ρ	
Density of gas	ρ_g	kg/m^3
Density of the porous medium	ρ_m	kg/m^3
Density of armor stones	ρ_r	kg/m^3
Density of solid	ρ_s	kg/m^3

Density of water	ρ_w	kg/m^3
Effective normal stress	σ'_n	kN/m^2
Effective vertical overburden stress	σ'_v	kN/m^2
Shear stress	τ	kN/m^2
Shear strength	$\bar{\tau}$	kN/m^2
Effective friction angle	ϕ'	$\circ$
Material stiffness tensor	$\boldsymbol{C}$	kN/m^2
Effective cohesion	c'	kN/m^2
Critical depth	d_{crit}	m
Armour layer thickness	d_D	m
Unconstrained stiffness modulus	E_S	MN/m^2
Limit state function	g	
Gravity	$\boldsymbol{g}$	m/s^2
Bow wave height	H_{bow}	m
Stern wave height	H_{stern}	m
Indicator function	I	
Effective bulk modulus of the pore fluid	K'	MN/m^2
Bulk modulus of water	K_w	MN/m^2
Hydraulic conductivity	k	m/s
Harmonic mean of hydraulic conductivity	k_{eff}	m/s
Random slice length	L	m
Number of simulations	N	
Number of slices	n	
Porosity of the armour stone layer	n_r	
Porosity of the solid material	n_s	
Pore pressure	p	kN/m^2
Atmospheric pressure	p_a	kN/m^2
Probability of failure	p_f	
Gas pressure	p_g	kN/m^2
Mean of the hydrostatic pore pressure over depth	$\overline{p_w}$	kN/m^2
Seepage velocity	$\boldsymbol{q}$	m/s
Saturation	S	
Time	t	s
Drawdown time	t_a	s
Displacement	$\boldsymbol{u}$	m
Drawdown height	z_a	m
Vector of (random) variables	$\boldsymbol{v}$	
Depth	y	m
Thickness of soil layer under consideration	y^*	m
Depth perpendicular to slope	z	m

References

Arnold, P. and Hicks, M. A. (2011): A stochastic approach to rainfall-induced slope failure. Vogt, N., Schuppener, B., Straub, D. and Brau, G. (eds.), Proceedings of the 3rd International Symposium on Geotechnical Safety and Risk, ISGR 2011, pp. 107-115.

Biot, M. (1956): General solutions of the equations of elasticity and consolidation for a porous material. pp. 91-96.

Cai, J.-S., Yan, E.-C., Yeh, T.-C. J., Zha, Y.-Y., Liang, Y., Huang, S.-Y., Wang, W.-K. and Wen, J.-C. (2017): Effect of spatial variability of shear strength on reliability of infinite slopes using analytical approach. Computers and Geotechnics, 81:77-86. https://doi.org/10.1016/j.compgeo.2016.07.012.

Cho, S. E. (2014): Probabilistic stability analysis of rainfall-induced landslides considering spatial variability of permeability. Engineering Geology, 171:11-20. https://doi.org/10.1016/j.enggeo.2013.12.015.

Clifton, P. M. and Neuman, S. P. (1982): Effects of kriging and inverse modeling on conditional simulation of the avra valley aquifer in southern arizona. Water Resources Research 18(4):1215-1234. https://doi.org/10.1029/WR018i004p01215.

Cooley, J. W. and Tukey, J. W. (1965): An algorithm for the machine calculation of complex fourier series. Mathematics of Computation, 19(90),:297. https://doi.org/10.1090/S0025-5718-1965-0178586-1.

Davis, M. W. (1987): Production of conditional simulations via the lu decomposition of the covariance matrix. Mathematical Geology, 19(2):91-98. https://doi.org/10.1007/BF00898189

DIN EN 1997-1:2014-03: Eurocode 7: Geotechnical design – Part 1: General rules; German version EN 1997-1:2004 + AC:2009 + A1:2013.

EAU (2012): Empfehlungen des Arbeitsausschusses "Ufereinfassungen" Häfen und Wasserstraßen [Recommendations of the Committee for Waterfront Structures] (11. ed.). Ernst & Sohn.

Ewers, J., Sorgatz, J. and Montenegro, H. (2017): Laborversuche und gekoppelte Berechnungen zur Untersuchung von Porenwasserüberdrücken infolge schneller Wasserstandsabsenkungen [Investigation on excess pore pressures due to rapid drawdown - laboratory tests and coupled simulations]. Deutsche Gesellschaft für Geotechnik e.V. (ed.), Fachsektionstage Geotechnik der Deutschen Gesellschaft für Geotechnik.

Fenton, G. A. and Vanmarcke, E. H. (1990): Simulation of random fields via local average subdivision. Journal of Engineering Mechanics, 116(8):1733-1749. https://doi.org/10.1061/(ASCE)0733-9399(1990)116:8(1733).

GBB (2010): Grundlagen zur Bemessung von Böschungs- und Sohlensicherungen an Binnenwasserstraßen (GBB) [BAW Code of Practice Principles for the Design of Bank and Bottom Protection for Inland Waterways]. BAWMerkblatt.

Gersch, W. and Yonemoto, J. (1977): Parametric time series models for multivariate EEG analysis. Computers and Biomedical Research, 10(2):113-125. https://doi.org/10.1016/0010-4809(77)90029-5.

Gesing, C. (2010): Hydraulische Belastungen am Ufer aus Schifffahrt und Abfluss [Hydraulic loads on the bank as a result of shipping and discharge]. Bundesanstalt fürWasserbau und Bundesanstalt für Gewässerkunde (eds.), Alternative technisch-biologische Ufersicherungen an Binnenwasserstraßen - Wirkungsweise, Belastbarkeit, Anwendungsmöglichkeiten, pp. 7-14.

Griffiths, D. V. and Fenton, G. A. (2007): Probabilistic Methods in Geotechnical Engineering (1. ed.). CISM International Centre for Mechanical Sciences, No. 491. CISM.

Griffiths, D. V., Huang, J. and Fenton, G. A. (2011): Probabilistic infinite slope analysis. Computers and Geotechnics, 38(4):577-584. ttps://doi.org/10.1016/j.compgeo.2011.03.006.

JCCS (2001): Probabilistic Model Code: PART I. Joint Committee on Structural Safety.

Köhler, H. J. (1989): Messung von Porenwasserüberdrücken im Untergrund [Measurements of excess pore pressures in the subsoil]. Mitteilungsblatt der Bundesanstalt für Wasserbau (66).

Madsen, O. S. (1978): Wave-induced pore pressures and effective stresses in a porous bed. Géotechnique, 28(4):377-393. https://doi.org/10.1680/geot.1978.28.4.377.

MAR (2008): Merkblatt Anwendung von Regelbauweisen für Böschungs- und Sohlensicherungen an Binnenwasserstraßen (MAR) [BAW Code of Practice Use of Standard Construction Methods for Bank and Bottom Protection on Waterways]. BAWMerkblatt.

Matheron, G. (1973): The intrinsic random functions and their applications. Advances in Applied Probability, 5(03):439-468. https://doi.org/10.2307/1425829.

Montenegro, H. (2016): FuE-Abschlussbericht: Infiltrationsdynamik in Erdbauwerken [Infiltration dynamics in earth structures].

Phoon, K.-K., Prakoso, W. A., Wang, Y. and Ching, J. (2016): Uncertainty representation of geotechnical design parameters. Phoon, K.-K. and Retief, J.V. (eds.), Reliability of Geotechnical Structures in ISO2394, pp. 49-87. London: CRC Press.

Rock Manual (2007): The Rock Manual. The use of rock in hydraulic engineering: The use of rock in hydraulic engineering. CIRIA, CUR, and CETMEF (eds.),Volume 683. London: CIRIA.

Santoso, A. M., Phoon, K.-K. and Quek, S.-T. (2011): Effects of soil spatial variability on rainfall-induced landslides. Computers & Structures, 89(11-12):893-900. https://doi.org/10.1016/j.compstruc.2011.02.016.

Terzaghi, K. (1943): Theoretical soil mechanics. J. Wiley & Sons Inc.

Vanmarcke, E. H. (1977): Probabilistic modeling of soil profiles. Journal of the Geotechnical Engineering Division, 103(11):1227-1246. https://doi.org/10.1061/AJGEB6.0000517.

Vanmarcke, E. H. (2010): Random fields. World Scientific Publ.

Vardon, P. J., Liu, K. and Hicks, M. A. (2016): Reduction of slope stability uncertainty based on hydraulic measurement via inverse analysis. Georisk: Assessment and Management of Risk for Engineered Systems and Geohazards, 10(3):223-240. https://doi.org/10.1080/17499518.2016.1180400.

Zhang, J., Huang, H. W., Zhang, L. M., Zhu, H. H. and Shi, B. (2014): Probabilistic prediction of rainfall-induced slope failure using a mechanics-based model. Engineering Geology, 168:129-140. https://doi.org/10.1016/j.enggeo.2013.11.005.

Zhou, A., Li, C.-Q. and Huang, J. (2016): Failure analysis of an infinite unsaturated soil slope. Geotechnical Engineering, 169(5):410-420. https://doi.org/10.1680/jgeen.15.00172.

Appendix

A.1 Initial and boundary conditions of the FE model

We assume that the initial fluid pressure and the solid displacements are known values:

$$\boldsymbol{u}(y, 0) = [0] \tag{A.1}$$

$$p(y, 0) = \gamma_w\, y \tag{A.2}$$

The boundary conditions specified at the top of the soil column (interface to the water surface) are:

$$\bar{\sigma}'\,(y = 0, t) = 0 \tag{A.3}$$

$$\bar{p}\,(y = 0, t) = \frac{z_a}{t_a}\,\gamma_w\, t \tag{A.4}$$

establishing an unrestricted deformable surface and pore pressure variations corresponding to a constant drawdown rate z_a/t_a The boundary conditions prescribed at the bottom of the soil column at a depth Y are:

$$\bar{u}\,(y = Y, t) = 0 \tag{A.5}$$

$$\bar{q}(y = Y, t) = 0 \tag{A.6}$$

which imply a rigid and impermeable layer at the base of the soil column.